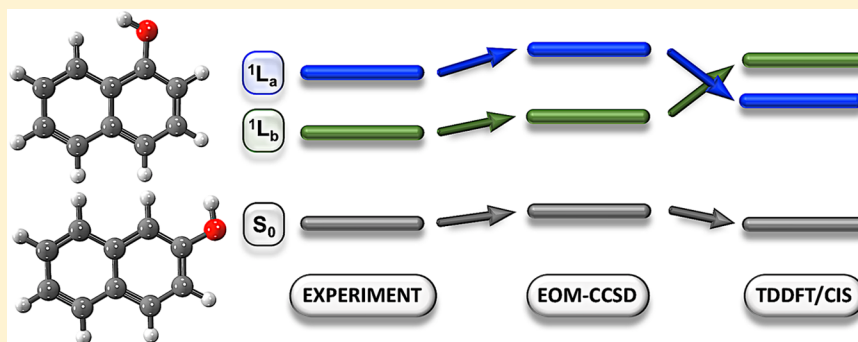# Can TDDFT Describe Excited Electronic States of Naphthol Photoacids? A Closer Look with EOM-CCSD

Atanu Acharya,*[ORCID] Subhajyoti Chaudhuri, and Victor S. Batista*[ORCID]

Department of Chemistry, Yale University, New Haven, Connecticut 06520, United States

S *Supporting Information*

ABSTRACT: The ^1L_b and ^1L_a excited states of naphthols are characterized by using time-dependent density functional theory (TDDFT), configuration interaction with singles (CIS), and equation-of-motion coupled cluster singles and doubles (EOM-CCSD) methods. TDDFT fails dramatically at predicting the energy and ordering of the ^1L_a and ^1L_b excited states as observed experimentally, while EOM-CCSD accurately predicts the excited states as characterized by natural transition orbital analysis. The limitations of TDDFT are attributed to the absence of correlation from doubly excited configurations as well as the inconsistent description of excited electronic states of naphthol photoacids revealed by excitation analysis based on the one-electron transition density matrix.

1. INTRODUCTION

The two low-lying excited states of acenes, called ^1L_a and ^1L_b as originally coined by Platt,[1] are common to all extended polyacenes. The transition dipole moments of the optically allowed $^1L_a \leftarrow S_0$ excitation and the optically forbidden $^1L_b \leftarrow S_0$ transition are approximately aligned along the short and long axes of the molecule, respectively.[2] In general, the ^1L_a state is optically bright and has significantly higher ionic character, as pointed out by several reports, while the ^1L_b state is dark and more covalent in nature.[2−6] It has also been suggested that the ^1L_a state of acenes has a charge-separated character.[3] The relative order of these two states depends on the size of the acene. For naphthalene and related molecules, the ^1L_b state is lower in energy than the ^1L_a state both in the gas phase and in solution.[7,8] Usually the ^1L_a state has a predominant contribution from the $\pi^* \leftarrow \pi$ (LUMO ← HOMO) excitation, whereas a combination of LUMO ← HOMO−1 and LUMO+1 ← HOMO excitations contribute to the ^1L_b state.[4,8]

Substituted naphthalenes have a wide range of applications. In particular, naphthols are photoacids since their acidity increases upon photoexcitation.[9,10] The OH substituent on the naphthalene ring also introduces further complexity in the electronic structure, with dramatically different effects with substitution of the 1- or 2-position of the aromatic ring (i.e., in 1-naphthol (1N) or 2-naphthol (2N), respectively; Figure 1). Although 1N and 2N have similar acidities in the ground
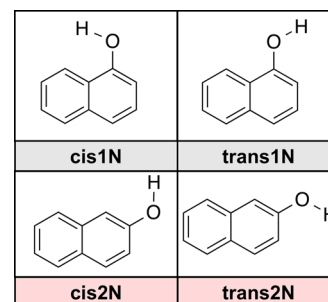

Figure 1. Isomers of naphthol under investigation in this study.

electronic state, their photoacidities are strikingly different. 1N is more photoacidic than 2N,[9,10] suggesting the involvement of excited states of different character in the stabilization of the conjugate base. Nevertheless, a molecular-level understanding of the photoacidity of naphthols remains controversial.[11−15]

Recently, a combined computational and experimental study invoked photoinduced electron transfer (ET) from naphthols to solvent molecules in the first solvation shell to explain the excited-state decay rates observed after photoexcitation.[16] Thus, a careful and rigorous analysis of the excited states is warranted.

Remarkably, although numerous experimental studies have been focused on the photoacidity of naphthols,[9,10,13,15] electronic characterization of the excited states involved has hitherto remained poorly understood.

The limitations of time-dependent density functional theory (TDDFT) in capturing ionic or charge-separated states have been reported and analyzed for numerous photochemical systems.[17−21] Hence, a significant underestimation of the energy predicted by TDDFT for the ^1L_a state is anticipated. In fact, for naphthols in low-dielectric media, the TDDFT underestimation of the ^1L_a energy is so high that the order of the ^1L_a and ^1L_b states is switched.[8,22] In polar solvents like DMSO, naphthols can be forced to undergo internal conversion (IC), bringing the ^1L_a state below ^1L_b at the excited-state minimum-energy configuration.[6] The ^1L_b state may be better described by TDDFT because of its more covalent character. Nevertheless, the order of energies predicted by TDDFT is usually incorrect to the extent that in the past they could be identified for vibrational analysis only through analysis of their distinct symmetries.[8,23] A similar switch in the order of the excited electronic states is observed for naphthalene, a difficulty that could be solved by using range-separated functionals.[24,25] However, correctly reproducing both of their individual excitation energies in polyacenes or similar molecules using TDDFT is a very complicated issue and may needed to be treated on a case-by-case basis.[25] Long-range-corrected functionals are usually the preferred choice when describing excited states with charge-separated character.[3,17,26,27] Unfortunately, such a solution is not transferable to naphthols[8,23] since the ionic character of the ^1L_a state is substantially reduced in naphthols compared with naphthalene because of intrinsic mixing of excited states induced by the OH substituent group. Regardless, the substituents affect the relative position of the ^1L_a and ^1L_b states quite drastically, as shown in the case of anthracene.[26] In addition, long-range-corrected functionals compromise the description of the ^1L_b state.[3] Recently, a study characterized ^1L_a and ^1L_b states of polyacenes and demonstrated that the natures of these states are highly sensitive to the functional used in the TDDFT calculations.[28]

Herein we show that the relative ordering of the excited electronic states and the energy spacing in naphthols is more complicated than in the case of naphthalene, particularly since the two lowest excited states of naphthols may not be purely ^1L_b and ^1L_a but rather an admixture of the two symmetries.[8,29] Therefore, we assess the capabilities and limitations of DFT methods compared with calculations based on equation-of-motion coupled cluster singles and doubles (EOM-CCSD),[30−38] which is a wavefunction based method that can be used for robust computation of excitation energies. In the EOM-CCSD formalism, the correlation effects are included in the form of higher-order excitations (singles and doubles). While the EOM-CCSD method is more expensive (because of its N^6 scaling) than DFT, it has been shown to be very accurate in describing the relative order and spacing of excited states since it includes correlations from higher-order excited configurations, which are often essential in excited-state calculations from a single-reference determinant (HF, DFT, etc.).

2. COMPUTATIONAL DETAILS

We analyzed the two possible isomers of naphthol, 1-naphthol (1N) and 2-naphthol (2N), including their two rotamers defining the two possible orientations ("cis" and "trans") of the OH group in the plane of the ring (Figure 1). Each molecule was optimized at the RI-MP2/cc-pVTZ level of theory in solution. For comparisons with experimental absorption spectra of naphthols in n-hexane,[8,23] we treated the solvent (n-hexane) as a dielectric continuum described by the C-PCM model[39] as implemented in the Q-Chem 5.0 software package.[40] The optimized geometries were used to compute the excitation energies for the ^1L_b and ^1L_a states at the TDDFT (with several different functionals), configuration interaction singles (CIS), and EOM-CCSD levels of theory. For efficiency in computation, we used the Cholesky decomposition of the electron-repulsion integral[41] in EOM-CCSD (as implemented in Q-Chem) with a Cholesky threshold of 10^{-3}. The basis set used in excited-state calculations was aug-cc-pVDZ. The performance of TDDFT was assessed using various functionals, including B3LYP,[42] B97-D3(BJ),[43,44] M06-2X-D3(0),[45] M06-L-D3(0),[45] CAM-B3LYP,[46] ωB97X-D,[47] and LRC-ωPBEh.[27] We also modified the B3LYP functional by varying the percentage of HF exchange. Natural transition orbital (NTO) analysis was carried out to characterize the natures of the individual excited states. It also allowed us to quantify the multiconfigurational natures of both excited states. Although EOM-CCSD is one of the most rigorous methods for computations of excitation energies, there is usually a 0.1−0.3 eV error associated with it.[48] The scaling of EOM-CCSD is on the order of $n \times N^6$, where N and n are the numbers of basis functions and excited states, respectively. To reach "chemical accuracy" with respect to absolute values of excitation energies, one needs to use EOM-CCSD with perturbative triples correction (EOM-CCSD(dT)),[49,50] which has a steeper scaling on the order of $n \times N^7$. However, the EOM-CCSD method is very efficient in describing relative spacings of excited states.[38] Another source of error in our computations may be attributed to the lack of explicit solute−solvent interactions. One way to circumvent the effect of the missing interactions is to use EOM-CCSD coupled with an effective fragment potential (EFP) approach with inclusion of dispersion and exchange-repulsion interactions between QM-EFP in the case of nonpolar solvents.[51] The effect of dispersion interactions between the solute and solvent, which is missing in the C-PCM model, may account for an error of ~0.3 eV in the solvatochromatic effects.[51] However, we anticipate the error to be systematic.

We compared the performances of CIS and TDDFT methods by analyzing the relative spacings of the ^1L_a and ^1L_b excited states compared with the results obtained with the EOM-CCSD method and experimental data. We also estimated the systematic errors in the excitation energies for the EOM-CCSD/C-PCM model with respect to the experimental results. NTO analysis was performed with EOM-CCSD/6-31+G(d) as implemented in Q-Chem.[40] Exciton analysis using the one-electron transition density matrix (1-TDM) was performed using the *libwfa* tool of Q-Chem[40] as described in refs 52−54.

3. RESULTS AND DISCUSSION

The transition dipole moments of the $^1L_b \leftarrow S_0$ and $^1L_a \leftarrow S_0$ transitions of 2N are at an angle relative to the long and short axes of the naphthalene ring, unlike the cases of 1N, naphthalene, and other acenes, which exhibit transition moments almost aligned along the axes of the molecule. Cis1N is most similar to naphthalene.[55] The molecular asymmetry due to the OH group at position 1 modifies the relative spacing and corresponding oscillator strengths of the excited states.[56] Nevertheless, the frontier orbitals of these

states preserve the symmetry of those in the parent naphthalene molecule.[8,23]

3.1. EOM-CCSD Characterization of the Excited States.

We begin with an assessment of errors in the excitation energies computed at the EOM-CCSD/aug-cc-pVDZ level by direct comparison to the corresponding experimental values (Table 1). We note that EOM-CCSD systematically overestimates the

Table 1. Comparison between Experimental[a] and EOM-CCSD-Derived[b] Excitation Energies

system	state	E_{ex} [eV]		error [eV]
		computed	exptl	
^1L_b	cis1N	4.30	3.87	0.43
	trans1N	4.33		0.46
^1L_b	cis2N	4.28	3.78	0.50
	trans2N	4.24		0.46
^1L_a	cis1N	4.69	4.27	0.42
	trans1N	4.79		0.52
^1L_a	cis2N	5.03	4.54	0.49
	trans2N	4.99		0.45

[a]Experimental absorption maxima were obtained from ref 8. [b]The EOM-CCSD excitation energies were computed using the aug-cc-pVDZ basis set.

excitation energies for both isomers (1N and 2N) by 0.42−0.52 eV. As discussed in Computational Details, this error can be attributed to the lack of triple excitations in EOM-CCSD (error ∼ 0.1−0.3 eV) and explicit solute−solvent interactions in the C-PCM model (error ∼ 0.3 eV). Additionally, one should keep in mind that computation of vibrational progressions is also necessary for unambiguous comparison between theoretical and experimental absorption spectra. However, such calculations require geometry optimizations in the excited state, which are computationally very expensive when performed with correlated methods. Additionally, previous studies have demonstrated that the maxima of electronic spectra in polyatomic molecules often align with the 0−0 transition as opposed to a vertical transition from vibrational ground state of the ground electronic state to a higher vibrational state of an electronic excited state.[57,58] Nevertheless, vibrational relaxation is required to bring the system to the vibrational ground state in the electronically excited state. Thus, vibrational relaxation can account for an additional red shift in the computed energies.[57−59]

For comparison of relevant energy gaps with experimental results, we define two energy parameters (gaps), ΔE_1 and ΔE_2, as follows:

$$\Delta E_1 = E(^1L_b)_{n_i} - E(^1L_a)_{n_i} \tag{1}$$

$$\Delta E_2 = E(1N)_{^1L_j} - E(2N)_{^1L_j} \tag{2}$$

where $n_i \in \{cis1N, trans1N, cis2N, trans2N\}$ and $j \in \{a, b\}$. ΔE_1 is the energy gap between the ^1L_b and ^1L_a states for each isomer and rotamer, whereas ΔE_2 quantifies the energy difference between 1N and 2N in the ^1L_b or ^1L_a state. Experimentally, it was observed that ^1L_b is lower than ^1L_a for all isomers and rotamers of naphthols. In addition, 2N is lower than 1N in the ^1L_b state but higher in the ^1L_a state. Thus, ΔE_1 is

always negative, while ΔE_2 is negative for ^1L_b and positive for ^1L_a.

Comparison of the experimental and EOM-CCSD values of ΔE_1 and ΔE_2 (Tables 2 and 3, respectively) shows that the

Table 2. Comparison of Values of the Energy Parameter ΔE_1 (eq 1) between EOM-CCSD[a] and Experiment

system	ΔE_1 [eV]
cis1N	−0.39
trans1N	−0.46
experiment (1N)	−0.42
cis2N	−0.75
trans2N	−0.75
experiment (2N)	−0.77

[a]Excitation energies were computed using the aug-cc-pVDZ basis set.

Table 3. Comparison of Values of the Energy Parameter ΔE_2 (eq 2) between EOM-CCSD[a] and Experiment

system	state	ΔE_2 [eV]
cis		−0.35
trans	^1L_b	−0.20
experiment		−0.27
cis		0.01
trans	^1L_a	0.09
experiment		0.07

[a]Excitation energies were computed using the aug-cc-pVDZ basis set.

EOM-CCSD method consistently reproduces the energy parameters in excellent agreement with the experiments. In contrast, section 3.2 shows the limitations of single-excitation-based methods (TDDFT and CIS). Hence, we analyze the properties of the excited states based on the EOM-CCSD calculations followed by a comparison with different TDDFT functionals (in following sections).

Table 4 summarizes the properties of the ^1L_b and ^1L_a states of naphthols in terms of the squared Frobenius norm (Ω) of the 1-electron transition density matrix (1-TDM) and the participation ratio of the natural transition orbitals (PR_{NTO}).[52,53] For an electronic transition of purely single-excitation character, $\Omega = 1$.[60] We note that Ω is less than 1 (0.77 to 0.79) for both excited states in all of the isomers and rotamers. This indicates contributions from double excitations for both states. However, the deviation from pure single-excitation character is not quite drastic (only about ∼21−23%) as presented for some cases.[60−62] If an electronic transition can be described purely by one NTO pair, $PR_{NTO} = 1$, while $PR_{NTO} = 2$ indicates that two NTO pairs are required to describe the transition correctly. PR_{NTO} analysis of these excited states suggests that for 1N rotamers, ^1L_b involves two individual transitions ($PR_{NTO} \sim 2$). This observation is also evident from the weights of each transition in Figure 2. However, ^1L_a states can be mostly described by one NTO pair with some contribution from a second pair. We can quantify the contribution of biconfigurational character (Δ_{2p}) of each state as follows:

$$\Delta_{2p} = \begin{cases} (PR_{NTO} - 1) \times 100\%, & 1 < PR_{NTO} \leq 2 \\ (3 - PR_{NTO}) \times 100\%, & 2 < PR_{NTO} \leq 3 \end{cases} \tag{3}$$
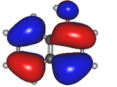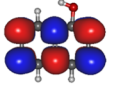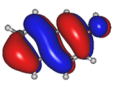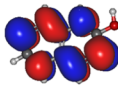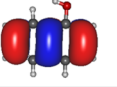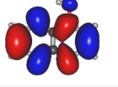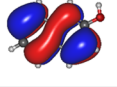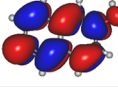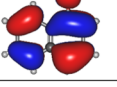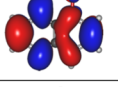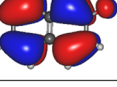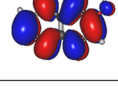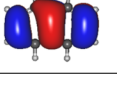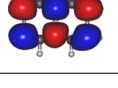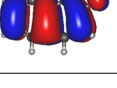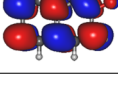
Figure 2. Leading NTOs involved in the first two excited states of 1N and 2N with isovalue = 0.02. For clarity we show only the results for the cis rotamers.

Table 4. Excited-State Properties of Naphthols Obtained Using EOM-CCSD Methods[a]

system	state	E_{ex} (computed) [eV]	Ω	PR_{NTO}	Δ_{2p} [%]
cis1N	^1L_b	4.30	0.77	2.00	100
	^1L_a	4.69	0.79	1.14	14
trans1N	^1L_b	4.33	0.77	2.01	99
	^1L_a	4.79	0.79	1.17	17
cis2N	^1L_b	4.28	0.77	1.81	81
	^1L_a	5.03	0.79	1.32	32
trans2N	^1L_b	4.24	0.77	1.76	76
	^1L_a	4.99	0.79	1.30	30

[a]Excitation energies were computed using the aug-cc-pVDZ basis set, and NTO analysis was performed at the EOM-CCSD/6-31+G(d) level.

Figure 2 shows the NTO pairs involved in the $^1L_b \leftarrow S_0$ and $^1L_a \leftarrow S_0$ transitions for cis rotamers. We observed that two NTO pairs with comparable weights are involved in the $^1L_b \leftarrow S_0$ transition. We also note similar behavior for the trans rotamers (see the Supporting Information). From Table 4 we see that the $^1L_a \leftarrow S_0$ transition in 1N can be described predominantly by one NTO pair, with contributions of only 14−17% from additional transitions. In the case of 2N, the $^1L_b \leftarrow S_0$ transitions deviate from purely biconfigurational character by 19−24%, whereas the biconfigurational contribution in $^1L_a \leftarrow S_0$ becomes even more significant (30−32% vs 14−17% in 1N).

3.2. Performance of TDDFT and CIS. Figures 3 and 4 assess the performance of TDDFT, as implemented with various hybrid and long-range-corrected functionals, by comparing values of the energy parameters with experimental data. In addition, we always compare energies/properties computed using the same basis set for both TDDFT and EOM-CCSD to eliminate basis set dependence from our comparisons of the excitation energies. The relevant states are identified in terms of the frontier orbitals involved in the electronic transitions, as reported by Xiao et al.[8] We note that TDDFT fails to predict the experimental values of ΔE_1 even when implemented in terms of range-separated/long-range-corrected functionals such as CAM-B3LYP, ωB97X-D, and LRC-ωPBEh. In fact, range-separated/long-range-corrected functionals predict ΔE_1 values with the wrong sign, artificially flipping the order of the two excited states. The CIS calculations (reference state is HF) also misplace the ^1L_a state lower in energy than the ^1L_b state. These limitations of the TDDFT and CIS methods are further investigated in the next section. Nevertheless, we do observe a good description of the ^1L_a state in cis1N using CIS, suggesting that the state is most ionic in nature. CIS is able to describe it properly since it has 100% HF exchange. We also note that all of the methods including EOM-CCSD reproduce similar trends for the cis and trans rotamers.

Experimentally it is observed that 2N is more stable than 1N in the ^1L_b state, resulting in a positive value of ΔE_2. However, TDDFT fails dramatically in predicting the correct order of the energy levels. The errors are comparable for all of the DFT functionals. The maximum error is observed for the ^1L_b states described by the M06-2X-D3 functional, which has the highest percentage of HF exchange (54%).[45] The origin of the error can be traced back to the nature of the excitations, which have significantly different amounts of multiconfigurational character for 1N and 2N (see Table 4). Therefore, the TDDFT errors are different and do not cancel out.

The performance of DFT functionals often depends critically on the percentage of HF exchange. Therefore, we investigated the sensitivity of the excitation energies (Figure 5a) and the predicted values of ΔE_1 for functionals with various amounts of short-range HF exchange. The percentage of HF exchange in B3LYP[42] (20% HF exchange + 8% Slater LSDA exchange + 72% B88 GGA exchange + 81% LYP GGA correlation + 19% VWN1RPA correlation) was systematically increased, and the total exchange was adjusted with reduced B88 GGA exchange. For example, B3LYP with 40% HF exchange refers to (40% HF + 8% Slater LSDA + 52% B88 GGA exchange + 81% LYP GGA correlation + 19% VWN1RPA correlation). Figure 5c shows that the error in computed excitation energy of the ^1L_a state decreases monotonically with increasing percentage of HF exchange, while the error in the ^1L_b state increases. Likewise, with a reduction in the percentage of HF exchange, the error in the ^1L_b state can be reduced while the description of the ^1L_a state is compromised. If one is interested in only one these

Figure 3. Comparison of the performances of EOM-CCSD and several DFT functionals with experiments. All of the calculations were performed using the aug-cc-pVDZ basis set. (a) Excitation energies of the ^1L_b and ^1L_a states from the ground state for (top) cis and (bottom) trans rotamers. (b) Energy difference ΔE_1 (see eq 1) for (top) cis and (bottom) trans rotamers. (c) Experimental UV−vis absorption spectra of 1N and 2N in *n*-hexane (ref 8). Relevant energy differences are highlighted.
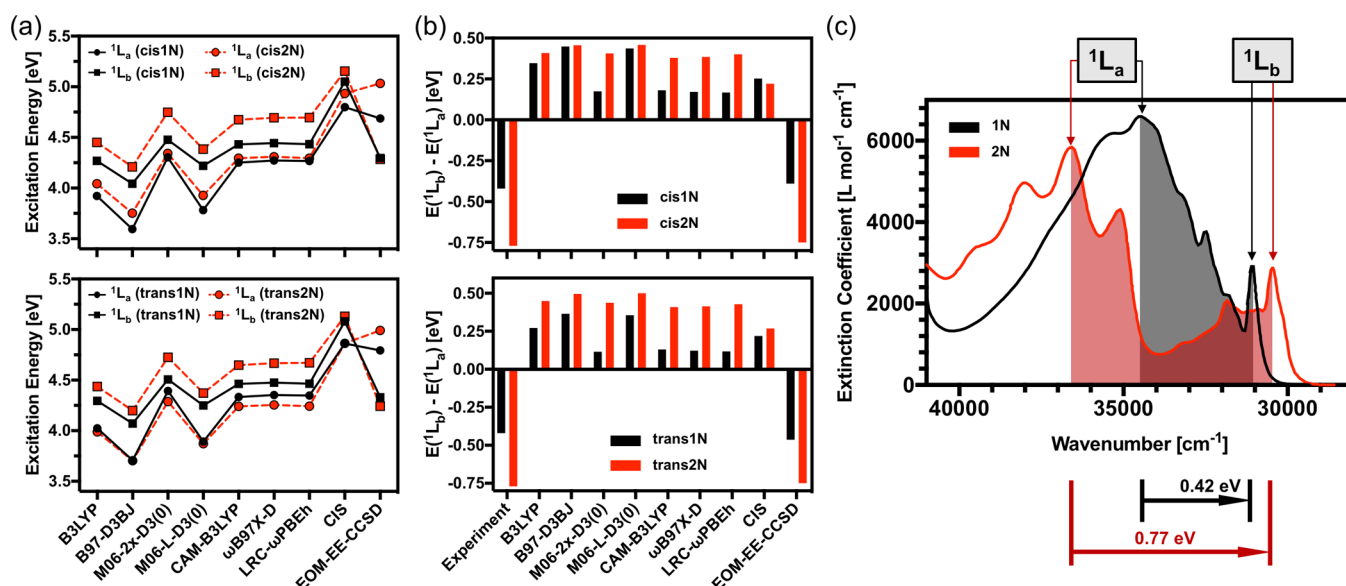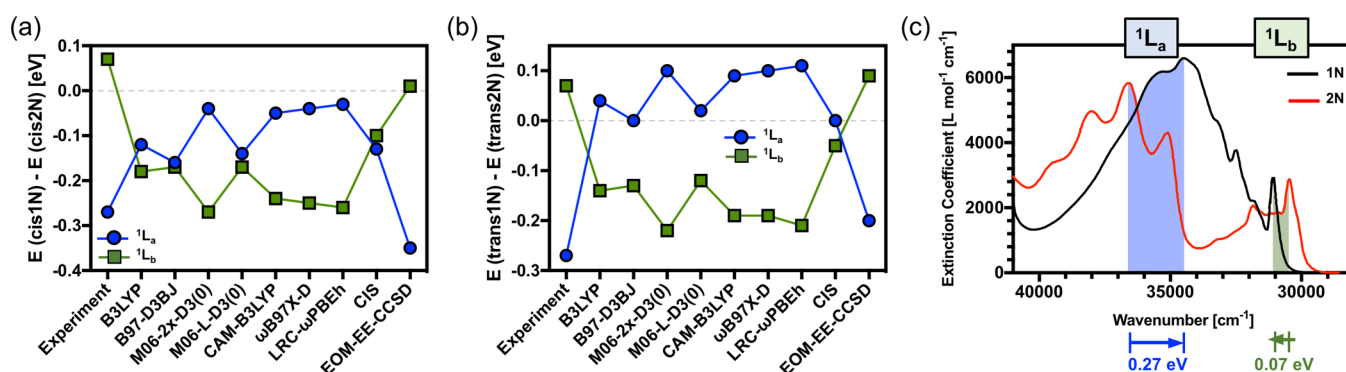

Figure 4. Comparison of the performances of EOM-CCSD and several DFT functionals with experiments. All of the calculations were performed using the aug-cc-pVDZ basis set. (a, b) Energy difference ΔE_2 (see eq 2) for (a) cis and (b) trans rotamers. (c) Experimental UV−vis absorption spectra of 1N and 2N in *n*-hexane(ref 8). Relevant energy differences are highlighted.

excited states, the accuracy in the excitation energy may be modified by varying the short-range HF exchange. However, Figure 5c also reveals that for a fixed percentage of HF exchange, the absolute error for 2N is always higher than that for 1N.

Because of the different accuracies of the ^1L_a and ^1L_b energies for any percentage of HF exchange, the accuracy in the spacing of these two states cannot be improved significantly by changing the percentage of HF exchange (Figure 5b). The most notable difference between the TDDFT and EOM-CCSD treatments of excited states is that the EOM-CCSD method includes double excitations. Another difference that might play a crucial role is the reference state. Usually an HF Slater determinant is the reference for the EOM-CCSD method, while TDDFT employs the DFT reference state. Therefore, we studied the accuracy of EOM-CCSD excited-state calculations based on the DFT/B3LYP reference state. Also, we compared the excitation energies obtained from TDHF and TDDFT. As expected, the TDHF results are very close to those for TD-B3LYP with 80% HF exchange. Table 5 shows that the EOM-CCSD results are quite insensitive to changes in the reference

state (the highest error is 0.04 eV), with the DFT and HF reference states giving comparable results at the EOM-CCSD level. In addition, Table 4 reveals a significant amount of biconfigurational character of ^1L_b, which is manifested in higher correlation in these states compared with the parent naphthalene molecule.[54] Further exciton analysis is warranted to elucidate this issue.

4. EXCITON ANALYSIS USING 1-TDM

The exciton analysis was performed using 1-TDM since it is orbital-invariant.[52,60,63] Before analysis of the exciton properties, the errors in the absolute excitation energies computed by TDDFT with various functionals should be noted. Table 6 shows that the errors in the excitation energies computed using B3LYP for the ^1L_a state are quite high because of the paucity of HF exchange, while the errors for the ^1L_b state are quite small for the 1N rotamers. Table 4 shows that there is significant mixing of the ^1L_a and ^1L_b states in the 2N rotamers. Thus, one might expect higher errors for the 2N rotamers in both excited states when using B3LYP.
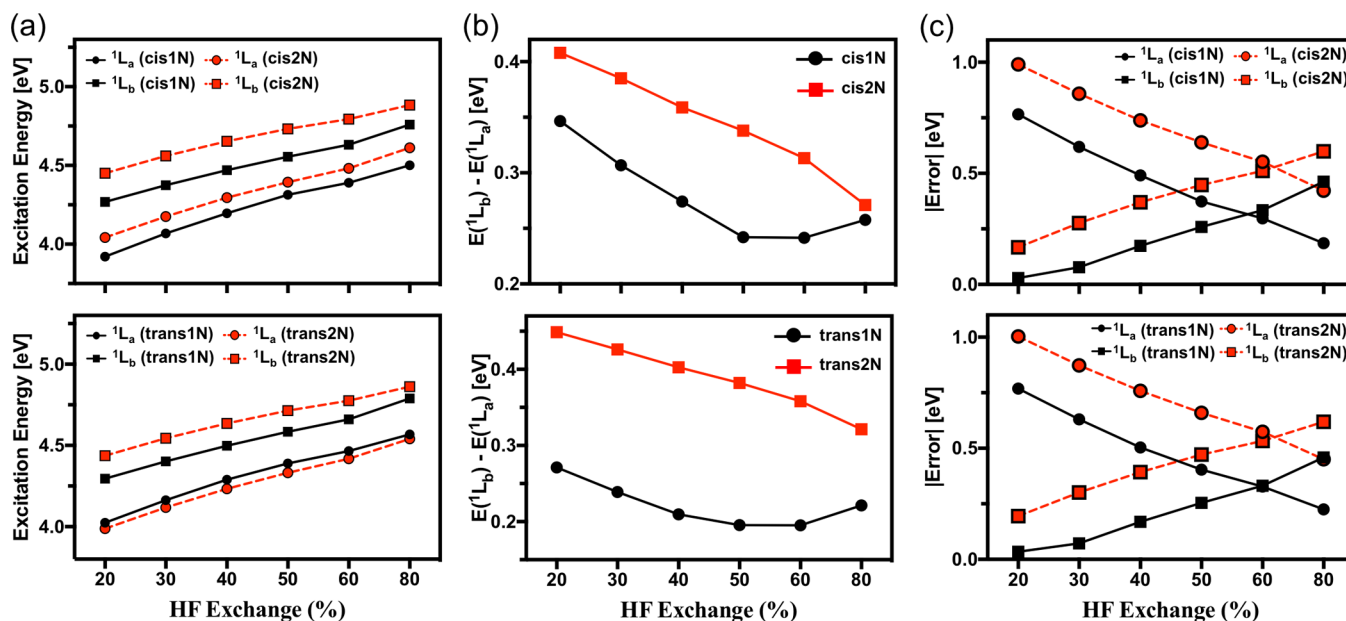
Figure 5. Effect of percentage of HF exchange in the functional on the excitation energies and energy difference ΔE_1 (see eq 1). The trend in performance with respect to varying % HF exchange is studied. All of the calculations were performed using the aug-cc-pVDZ basis set. (a) Excitation energies of the ^1L_b and ^1L_a states from the ground state for (top) cis and (bottom) trans rotamers with respect to varying % HF exchange. (b) Energy difference ΔE_1 (see eq 1) for (top) cis and (bottom) trans rotamers with respect to varying % HF exchange. (c) Absolute errors in the respective excitation energies with respect to varying % HF exchange. The absolute error is estimated with respect to EOM-CCSD as |Error| = | E^{ex}_{state}(EOM-CCSD) $- E^{ex}_{state}$(TDDFT)|.

Table 5. Comparison of EOM-CCSD Excitation Energies Obtained Using HF and DFT Reference States and Comparison of TDDFT and TDHF Excitation Energies[a]

state	system	EOM-CCSD E_{ex} [eV]			TDDFT E_{ex} [eV]	TDHF E_{ex} [eV]
		HF ref	B3LYP ref	error		
^1L_b	cis1N	4.34	4.33	0.01	4.76	4.83
	cis2N	4.34	4.33	0.00	4.88	4.91
	trans1N	4.37	4.37	0.00	4.79	4.86
	trans2N	4.30	4.28	0.02	4.86	4.88
^1L_a	cis1N	4.86	4.82	0.04	4.50	4.49
	cis2N	5.20	5.20	0.00	4.61	4.63
	trans1N	4.98	4.99	−0.01	4.57	4.55
	trans2N	5.14	5.13	0.01	4.54	4.56

[a]EOM-CCSD excitation energies were computed using the 6-31+G(d) basis set. TDDFT and TDHF excitation energies were computed using the aug-cc-pVDZ basis set.

From Table 6, we also notice that while the error in the energy of the ^1L_a state can be reduced (relative to B3LYP) by using range-separated/long-range-corrected functionals, the error in the energy of ^1L_b significantly increases, in agreement with previously reported results for naphthalene.[5,24,27]

The ionic characters of these excited states were computed, and the results are summarized in Table 7 in terms of the electron−hole separation ($|\langle r_e - r_h \rangle|$; see Figure 6a). The different behavior of the electron−hole separation in the ^1L_a and ^1L_b states has also been reported for several acenes, providing a strategy to quantify the ionic/covalent character of the state.[5,54,61,62]

From the EOM-CCSD results, we observe that ^1L_a states in 1N have significantly higher ionic character compared with the other isomers. Particularly noticeable is the cis1N state, which

Table 6. Errors Involved in Excitation Energies Using Different DFT Functionals Estimated with Respect to EOM-CCSD as $Error_{ex} = E^{EOM-CCSD}_{ex} - E^{TDDFT}_{ex}$ [a]

state	system	$Error_{ex}$ [eV]		
		B3LYP	CAM-B3LYP	ωB97X-D
^1L_a	cis1N	0.88	0.54	0.51
	cis2N	1.10	0.83	0.82
	trans1N	0.89	0.56	0.54
	trans2N	1.10	0.84	0.82
^1L_b	cis1N	0.02	−0.15	−0.16
	cis2N	−0.16	−0.40	−0.42
	trans1N	0.03	−0.15	−0.17
	trans2N	−0.19	−0.41	−0.43

[a]All of the calculations were performed using the 6-31+G(d) basis set.

Table 7. Comparison of TDDFT and EOM-CCSD Derived Electron-Hole Separations[a]

state	system	$|\langle r_e - r_h \rangle|$ [Å]			
		B3LYP	CAM-B3LYP	ωB97X-D	EOM-CCSD
^1L_a	cis1N	1.25	0.87	0.86	1.05
	cis2N	0.51	0.35	0.35	0.28
	trans1N	0.97	0.59	0.59	0.78
	trans2N	0.54	0.37	0.37	0.33
^1L_b	cis1N	0.39	0.26	0.25	0.20
	cis2N	0.14	0.14	0.14	0.20
	trans1N	0.28	0.22	0.23	0.12
	trans2N	0.17	0.17	0.17	0.21

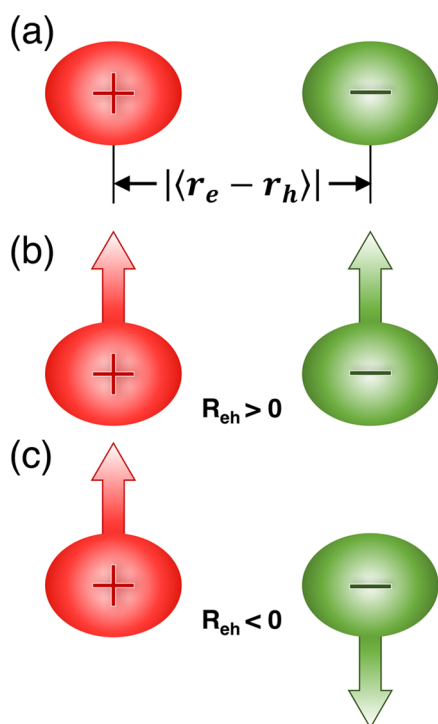[a]All of the calculations were performed using the 6-31+G(d) basis set.

Figure 6. Illustration of the relevant parameters from exciton analysis. (a) Electron−hole separation, measured as the distance between their respective centers. (b) Positive electron−hole correlation coefficient R_{eh} (see eq 4), representing a bound exciton. (c) Negative electron−hole correlation coefficient R_{eh}, representing anticorrelated motion of the electron and hole.

exhibits the highest ionic character and has the closest resemblance to the parent naphthalene molecule. ^1L_b states are always found to be more covalent in nature.[3,62] For ^1L_a states, B3LYP overestimates the ionic character for all of the isomers, whereas CAM-B3LYP and ωB97X-D underestimate the ionic character of 1N and slightly overestimate that of 2N. Other functionals slightly overestimate the ionic character of 1N and slightly underestimate it in the case of 2N for ^1L_b state. However, these variations in exciton properties are not related to the variations in 1-TDM, since from Table 8 we notice that the differences between the respective 1-TDM norms Ω computed with TDDFT and EOM-CCSD (0.21−0.23) are very similar for all of the isomers of a specific state (^1L_a or ^1L_b).

Table 8. Comparison of 1-TDM Norms Ω Computed with TDDFT and EOM-CCSD[a]

state	system	Ω			
		B3LYP	CAM-B3LYP	ωB97X-D	EOM-CCSD
^1L_a	cis1N	1.0	1.0	1.0	0.79
	cis2N	1.0	1.0	1.0	0.79
	trans1N	1.0	1.0	1.0	0.79
	trans2N	1.0	1.0	1.0	0.79
^1L_b	cis1N	1.0	1.0	1.0	0.77
	cis2N	1.0	1.0	1.0	0.77
	trans1N	1.0	1.0	1.0	0.77
	trans2N	1.0	1.0	1.0	0.77

[a]All of the calculations were performed using the 6-31+G(d) basis set.

The difference between TDDFT and EOM-CCSD in regard to the norm of 1-TDM reflects the deviation from purely single-excitation character in the nature of the excited state. The deviation is not drastic enough to be solely responsible for the dramatically poor performance of TDDFT. In contrast to TDDFT, the doubly excited configurations in EOM-CCSD provide correlation for the predominantly singly excited states in addition to capturing the contributions of any double-excitation character in the excited states.

Table 9 summarizes the NTO participation ratio (PR_{NTO}) values for both excited states for all of the isomers using

Table 9. Comparison of NTO Participation Ratios (PR_{NTO}) Obtained with TDDFT and EOM-CCSD[a]

state	system	PR_{NTO}			
		B3LYP	CAM-B3LYP	ωB97X-D	EOM-CCSD
^1L_a	cis1N	1.09	1.11	1.11	1.14
	cis2N	1.19	1.30	1.30	1.32
	trans1N	1.11	1.15	1.15	1.17
	trans2N	1.16	1.25	1.26	1.30
^1L_b	cis1N	1.77	1.84	1.84	2.00
	cis2N	1.65	1.55	1.53	1.81
	trans1N	1.76	1.75	1.73	2.01
	trans2N	1.71	1.61	1.59	1.76

[a]All of the calculations were performed using the 6-31+G(d) basis set.

TDDFT and EOM-CCSD. We observe that the ^1L_a states are well-described (error ∼ 0.02−0.05) by CAM-B3LYP and ωB97X-D, whereas a larger error in PR_{NTO} (0.05−0.14) is associated with B3LYP. Additionally, the B3LYP error is higher for 2N than for 1N. However, PR_{NTO} for ^1L_b states elucidates one of the reasons behind the compromised accuracy of the ^1L_b state when range-separated/long-range-corrected functionals are used. Furthermore, the comparisons with EOM-CCSD results listed in Table 9 show that the errors in PR_{NTO} for ^1L_b states are lower for B3LYP (0.05−0.25) compared with CAM-B3LYP (0.15−0.26) and ωB97X-D (0.16−0.30).

The long-range electron−hole correlation parameter (R_{eh}) can be computed as follows:[4,54,62]

$$R_{eh} = \frac{\langle \mathbf{r}_h \cdot \mathbf{r}_e \rangle - \langle \mathbf{r}_h \rangle \cdot \langle \mathbf{r}_e \rangle}{\sigma_h \sigma_e} \quad (4)$$

where σ_h and σ_e are the root-mean-square sizes of the electron and hole, respectively, in the exciton. The values of R_{eh} are in the range [−1, 1]. A positive value of R_{eh} represents a bound exciton with correlated motion of the electron and hole in the exciton picture (see Figure 6b). A negative value of R_{eh} corresponds to anticorrelated motion of the electron and the hole (see Figure 6c). $R_{eh} = 0$ indicates a lack of correlation between the electron and the hole. Typically, small values of R_{eh} are observed for small molecules.[4,28]

Table 10 summarizes the R_{eh} values for both excited states in all of the isomers using TDDFT and EOM-CCSD. The observed electron−hole correlations are similar to the values obtained for naphthalene.[28,54] More importantly, in the B3LYP description of the ^1L_a state there appears to be an unbound exciton, which does not agree with the EOM-CCSD description. CAM-B3LYP and ωB97X-D improve the description of this state but fail to be consistent across isomers. Similar negative R_{eh} values are also reported for naphthalene using

Table 10. Comparison of Electron−Hole Correlation Parameter (R_{eh}) Values for TDDFT and EOM-CCSD[a]

state	system	R_{eh}			
		B3LYP	CAM-B3LYP	ωB97X-D	EOM-CCSD
^1L_a	cis1N	−0.03	0.03	0.03	0.03
	cis2N	−0.01	0.08	0.09	0.02
	trans1N	−0.04	0.04	0.04	0.03
	trans2N	−0.01	0.08	0.08	0.02
^1L_b	cis1N	0.04	0.12	0.12	0.15
	cis2N	0.00	0.07	0.07	0.14
	trans1N	0.04	0.11	0.11	0.15
	trans2N	0.00	0.08	0.08	0.14

[a]All of the calculations were performed using the 6-31+G(d) basis set.

B3LYP.[28] Additionally, it is known that the use of CAM-B3LYP restores the slightly bound exciton picture of these states for naphthalene.[28] Our observation correlates with the reduced error for CAM-B3LYP and ωB97X-D compared with B3LYP. Additionally, our results correlate with the increased error in 2N compared with 1N, following the trend observed in PR_{NTO}, since the errors (relative to EOM-CCSD) in R_{eh} are higher in 2N than in 1N for all of the functionals. R_{eh} for the ^1L_b state is about 5 times higher than R_{eh} observed for ^1L_a. Thus, exciton analysis based on 1-TDM highlights the reasons behind the apparent failure of TDDFT in the context of the ^1L_a and ^1L_b states of naphthols. The problem of poor description of the electronically excited states can be attributed to several factors: the lack of correlations from double excitations, the incomplete picture of the collective nature of excitation induced by mixing of the two excited states, and incorrect electron−hole correlation effects in TDDFT.

5. SUMMARY AND CONCLUSIONS

We have analyzed the two lowest excited states of 1- and 2-naphthol using DFT and EOM-CCSD methods for electronic structure calculations. EOM-CCSD correctly reproduces the experimental ordering and relative spacing of the excited states for all isomers and rotamers, although it systematically overestimates the absolute excitation energies. In contrast, TDDFT fails to predict the correct energy order of the excited states, irrespective of the choice of functional or percentage of HF exchange. Consequently, the relative spacings of the excited states are not properly described by TDDFT. The errors introduced by TDDFT in the calculations of the ^1L_b and ^1L_a energies are different because of the different characters of the two states. By changing the percentage of HF exchange, one can reduce the error for a particular state, but only at the expense of increasing the error for the other. The errors in TDDFT are higher for 2N than for 1N since the mixing of excited states is higher for 2N, as quantified by the parameter Δ_{2p} (also see Table 9). Additionally, the electron−hole correlation is found to be a very important metric for correct characterization of excited states when comparing different methods. In particular, the inconsistency of TDDFT is clearly highlighted by such a metric. In addition, we find that long-range-corrected functionals fail to remedy the deficiencies of TDDFT as applied to the description of the excited states of naphthols. The failure of range-separated/long-range-corrected functionals is shown to stem from higher error in the collectivity index (as quantified by PR_{NTO}) and inconsistent correlation in ^1L_b states.

We conclude that the EOM-CCSD method provides a rigorous way of characterizing the excited states of naphthols, revealing the true nature of the excited states in term of exciton parameters. Current DFT functionals dramatically fall short in this context. Relying on error cancellation while studying trends using TDDFT excitation energies can lead to erroneous conclusions since the errors are not systematic and depend on the nature of the excited state. We anticipate that the conclusions drawn in this study will be transferable to other photoacids where similar states play a pivotal role.

■ ASSOCIATED CONTENT

Ⓢ Supporting Information

The Supporting Information is available free of charge on the ACS Publications website at DOI: 10.1021/acs.jctc.7b01101.

Optimized geometries of naphthols, NTOs for trans isomers, effect of the basis set on the excitation energies, and exciton analysis of naphthalene using CAM-B3LYP (PDF)

■ AUTHOR INFORMATION

Corresponding Authors
*E-mail: atanu.acharya@yale.edu (A.A.).
*E-mail: victor.batista@yale.edu (V.S.B.).

ORCID Ⓘ
Atanu Acharya: 0000-0002-6960-7789
Victor S. Batista: 0000-0002-3262-1237

Notes
The authors declare no competing financial interest.

■ REFERENCES

(1) Platt, J. R. Classification of spectra of cata-condensed hydrocarbons. *J. Chem. Phys.* **1949**, 17, 484−495.
(2) Grimme, S.; Parac, M. Substantial errors from time-dependent density functional theory for the calculation of excited states of large π systems. *ChemPhysChem* **2003**, 4, 292−295.
(3) Richard, R. M.; Herbert, J. M. Time-dependent density-functional description of the ^1L_a state in polycyclic aromatic hydrocarbons: Charge-transfer character in disguise? *J. Chem. Theory Comput.* **2011**, 7, 1296−1306.
(4) Plasser, F.; Thomitzni, B.; Bäppler, S. A.; Wenzel, J.; Rehn, D. R.; Wormit, M.; Dreuw, A. Statistical analysis of electronic excitation processes: Spatial location, compactness, charge transfer, and electron-hole correlation. *J. Comput. Chem.* **2015**, 36, 1609−1620.
(5) Wong, B. M.; Hsieh, T. H. Optoelectronic and excitonic properties of oligoacenes: Substantial improvements from range-separated time-dependent density functional theory. *J. Chem. Theory Comput.* **2010**, 6, 3704−3712.
(6) Messina, F.; Prémont-Schwarz, M.; Braem, O.; Xiao, D.; Batista, V. S.; Nibbering, E. T. J.; Chergui, M. Ultrafast solvent-assisted

electronic level crossing in 1-naphthol. *Angew. Chem., Int. Ed.* **2013**, *52*, 6871−6875.

(7) Biermann, D.; Schmidt, W. Diels-Alder reactivity of polycyclic aromatic hydrocarbons. 1. Acenes and benzologs. *J. Am. Chem. Soc.* **1980**, *102*, 3163−3173.

(8) Xiao, D.; Prémont-Schwarz, M.; Nibbering, E. T. J.; Batista, V. S. Ultrafast vibrational frequency shifts induced by electronic excitations: Naphthols in low dielectric media. *J. Phys. Chem. A* **2012**, *116*, 2775−2790.

(9) Pines, E.; Fleming, G. R. Self quenching of 1-naphthol. Connection between time-resolved and steady-state measurements. *Chem. Phys.* **1994**, *183*, 393−402.

(10) Tolbert, L. M.; Haubrich, J. E. Photoexcited proton transfer from enhanced photoacids. *J. Am. Chem. Soc.* **1994**, *116*, 10593−10600.

(11) Pines, D.; Nibbering, E. T. J.; Pines, E. Monitoring the microscopic molecular mechanisms of proton transfer in acid-base reactions in aqueous solutions. *Isr. J. Chem.* **2015**, *55*, 1240−1251.

(12) Granucci, G.; Hynes, J. T.; Millie, P.; Tran-Thi, T.-H. A theoretical investigation of excited-state acidity of phenol and cyanophenols. *J. Am. Chem. Soc.* **2000**, *122*, 12243−12253.

(13) Agmon, N.; Rettig, W.; Groth, C. Electronic determinants of photoacidity in cyanonaphthols. *J. Am. Chem. Soc.* **2002**, *124*, 1089−1096.

(14) Psciuk, B. T.; Prémont-Schwarz, M.; Koeppe, B.; Keinan, S.; Xiao, D.; Nibbering, E. T. J.; Batista, V. S. Correlating photoacidity to hydrogen-bond structure by using the local O-H stretching probe in hydrogen-bonded complexes of aromatic alcohols. *J. Phys. Chem. A* **2015**, *119*, 4800−4812.

(15) Pines, E.; Magnes, B.-Z.; Lang, M. J.; Fleming, G. R. Direct measurement of intrinsic proton transfer rates in diffusion-controlled reactions. *Chem. Phys. Lett.* **1997**, *281*, 413−420.

(16) Chaudhuri, S.; Rudshteyn, B.; Prémont-Schwarz, M.; Pines, D.; Pines, E.; Huppert, D.; Nibbering, E. T. J.; Batista, V. S. Ultrafast photo-induced charge transfer of 1-naphthol and 2-naphthol to halocarbon solvents. *Chem. Phys. Lett.* **2017**, *683*, 49−56.

(17) Dreuw, A.; Head-Gordon, M. Failure of time-dependent density functional theory for long-range charge-transfer excited states: the zincbacteriochlorin- bacteriochlorin and bacteriochlorophyll- spheroidene complexes. *J. Am. Chem. Soc.* **2004**, *126*, 4007−4016.

(18) Bernasconi, L.; Sprik, M.; Hutter, J. Time dependent density functional theory study of charge-transfer and intramolecular electronic excitations in acetone-water systems. *J. Chem. Phys.* **2003**, *119*, 12417−12431.

(19) Magyar, R. J.; Tretiak, S. Dependence of spurious charge-transfer excited states on orbital exchange in TDDFT: Large molecules and clusters. *J. Chem. Theory Comput.* **2007**, *3*, 976−987.

(20) Neugebauer, J.; Louwerse, M. J.; Baerends, E. J.; Wesolowski, T. A. The merits of the frozen-density embedding scheme to model solvatochromic shifts. *J. Chem. Phys.* **2005**, *122*, 094115.

(21) Lange, A.; Herbert, J. M. Simple methods to reduce charge-transfer contamination in time-dependent density-functional calculations of clusters and liquids. *J. Chem. Theory Comput.* **2007**, *3*, 1680−1690.

(22) Plusquellic, D. F.; Tan, X.-Q.; Pratt, D. W. Acid-base chemistry in the gas phase. the cis-and trans-2-naphthol·NH_3 complexes in their S_0 and S_1 states. *J. Chem. Phys.* **1992**, *96*, 8026−8036.

(23) Prémont-Schwarz, M.; Xiao, D.; Batista, V. S.; Nibbering, E. T. J. The O-H stretching mode of a prototypical photoacid as a local dielectric probe. *J. Phys. Chem. A* **2011**, *115*, 10511−10516.

(24) Lopata, K.; Reslan, R.; Kowalska, M.; Neuhauser, D.; Govind, N.; Kowalski, K. Excited-state studies of polyacenes: a comparative picture using EOMCCSD, CR-EOMCCSD(T), range-separated (LR/RT)-TDDFT, TD-PM3, and TD-ZINDO. *J. Chem. Theory Comput.* **2011**, *7*, 3686−3693.

(25) Prlj, A.; Sandoval-Salinas, M. E.; Casanova, D.; Jacquemin, D.; Corminboeuf, C. Low-lying $\pi\pi^*$ states of heteroaromatic molecules: A challenge for excited state methods. *J. Chem. Theory Comput.* **2016**, *12*, 2652−2660.

(26) Abou-Hatab, S.; Spata, V. A.; Matsika, S. Substituent effects on the absorption and fluorescence properties of anthracene. *J. Phys. Chem. A* **2017**, *121*, 1213−1222.

(27) Rohrdanz, M. A.; Martins, K. M.; Herbert, J. M. A long-range-corrected density functional that performs well for both ground-state properties and time-dependent density functional theory excitation energies, including charge-transfer excited states. *J. Chem. Phys.* **2009**, *130*, 054112.

(28) Mewes, S. A.; Plasser, F.; Dreuw, A. Communication: Exciton analysis in time-dependent density functional theory: How functionals shape excited-state characters. *J. Chem. Phys.* **2015**, *143*, 171101.

(29) Nishimoto, K. Electronic spectra and structure of α-and β-naphthol. *J. Phys. Chem.* **1963**, *67*, 1443−1446.

(30) Rowe, D. J. Equations-of-motion method and the extended shell model. *Rev. Mod. Phys.* **1968**, *40*, 153−166.

(31) Emrich, K. An extension of the coupled-cluster formalism to excited states (I). *Nucl. Phys. A* **1981**, *351*, 379−396.

(32) Geertsen, J.; Rittby, M.; Bartlett, R. J. The equation-of-motion coupled-cluster method: Excitation energies of Be and CO. *Chem. Phys. Lett.* **1989**, *164*, 57−62.

(33) Stanton, J. F.; Bartlett, R. J. The equation of motion coupled-cluster method. A systematic biorthogonal approach to molecular excitation energies, transition probabilities, and excited state properties. *J. Chem. Phys.* **1993**, *98*, 7029−7039.

(34) Comeau, D. C.; Bartlett, R. J. The equation-of-motion coupled-cluster method. Applications to open- and closed-shell reference states. *Chem. Phys. Lett.* **1993**, *207*, 414−423.

(35) Stolarczyk, L. Z.; Monkhorst, H. J. Coupled-cluster method with optimized reference state. *Int. J. Quantum Chem., Quantum Chem. Symp.* **1984**, *18*, 267−291.

(36) Sinha, D.; Mukhopadhyay, D.; Mukherjee, D. A note on the direct calculation of excitation-energies by quasi-degenerate MBPT and coupled-cluster theory. *Chem. Phys. Lett.* **1986**, *129*, 369−374.

(37) Stanton, J. F.; Gauss, J. A discussion on some problems associated with the quantum mechanical treatment of open-shell molecules. *Adv. Chem. Phys.* **2003**, *125*, 101−146.

(38) Krylov, A. I. Equation-of-motion coupled-cluster methods for open-shell and electronically excited species: The hitchhiker's guide to Fock space. *Annu. Rev. Phys. Chem.* **2008**, *59*, 433−462.

(39) Cossi, M.; Rega, N.; Scalmani, G.; Barone, V. Energies, structures, and electronic properties of molecules in solution with the C-PCM solvation model. *J. Comput. Chem.* **2003**, *24*, 669−681.

(40) Shao, Y.; Gan, Z.; Epifanovsky, E.; Gilbert, A. T. B.; Wormit, M.; Kussmann, J.; Lange, A. W.; Behn, A.; Deng, J.; Feng, X.; Ghosh, D.; Goldey, M.; Horn, P. R.; Jacobson, L. D.; Kaliman, I.; Khaliullin, R. Z.; Kus, T.; Landau, A.; Liu, J.; Proynov, E. I.; Rhee, Y. M.; Richard, R. M.; Rohrdanz, M. A.; Steele, R. P.; Sundstrom, E. J.; Woodcock, H. L., III; Zimmerman, P. M.; Zuev, D.; Albrecht, B.; Alguire, E.; Austin, B.; Beran, G. J. O.; Bernard, Y. A.; Berquist, E.; Brandhorst, K.; Bravaya, K. B.; Brown, S. T.; Casanova, D.; Chang, C.-M.; Chen, Y.; Chien, S. H.; Closser, K. D.; Crittenden, D. L.; Diedenhofen, M.; DiStasio, R. J., Jr.; Do, H.; Dutoi, A. D.; Edgar, R. G.; Fatehi, S.; Fusti-Molnar, L.; Ghysels, A.; Golubeva-Zadorozhnaya, A.; Gomes, J.; Hanson-Heine, M. W. D.; Harbach, P. H. P.; Hauser, A. W.; Hohenstein, E. G.; Holden, Z. C.; Jagau, T.-C.; Ji, H.; Kaduk, B.; Khistyaev, K.; Kim, J.; Kim, J.; King, R. A.; Klunzinger, P.; Kosenkov, D.; Kowalczyk, T.; Krauter, C. M.; Lao, K. U.; Laurent, A.; Lawler, K. V.; Levchenko, S. V.; Lin, C. Y.; Liu, F.; Livshits, E.; Lochan, R. C.; Luenser, A.; Manohar, P.; Manzer, S. F.; Mao, S.-P.; Mardirossian, N.; Marenich, A. V.; Maurer, S. A.; Mayhall, N. J.; Neuscamman, E.; Oana, C. M.; Olivares-Amaya, R.; O'Neill, D. P.; Parkhill, J. A.; Perrine, T. M.; Peverati, R.; Prociuk, A.; Rehn, D. R.; Rosta, E.; Russ, N. J.; Sharada, S. M.; Sharma, S.; Small, D. W.; Sodt, A.; Stein, T.; Stuck, D.; Su, Y.-C.; Thom, A. J. W.; Tsuchimochi, T.; Vanovschi, V.; Vogt, L.; Vydrov, O.; Wang, T.; Watson, M. A.; Wenzel, J.; White, A.; Williams, C. F.; Yang, J.; Yeganeh, S.; Yost, S. R.; You, Z.-Q.; Zhang, I. Y.; Zhang, X.; Zhao, Y.; Brooks, B. R.; Chan, G. K. L.; Chipman, D. M.; Cramer, C. J.; Goddard, W. A., III; Gordon, M. S.; Hehre, W. J.; Klamt, A.; Schaefer, H. F., III; Schmidt, M. W.; Sherrill, C. D.; Truhlar, D. G.; Warshel, A.;

Xu, X.; Aspuru-Guzik, A.; Baer, R.; Bell, A. T.; Besley, N. A.; Chai, J.-D.; Dreuw, A.; Dunietz, B. D.; Furlani, T. R.; Gwaltney, S. R.; Hsu, C.-P.; Jung, Y.; Kong, J.; Lambrecht, D. S.; Liang, W.; Ochsenfeld, C.; Rassolov, V. A.; Slipchenko, L. V.; Subotnik, J. E.; Van Voorhis, T.; Herbert, J. M.; Krylov, A. I.; Gill, P. M. W.; Head-Gordon, M. Advances in molecular quantum chemistry contained in the Q-Chem 4 program package. *Mol. Phys.* **2015**, *113*, 184−215.

(41) Epifanovsky, E.; Zuev, D.; Feng, X.; Khistyaev, K.; Shao, Y.; Krylov, A. I. General implementation of resolution-of-identity and Cholesky representations of electron-repulsion integrals within coupled-cluster and equation-of-motion methods: Theory and benchmarks. *J. Chem. Phys.* **2013**, *139*, 134105.

(42) Becke, A. D. Density-functional thermochemistry. III. The role of exact exchange. *J. Chem. Phys.* **1993**, *98*, 5648.

(43) Becke, A. D. Density-functional thermochemistry. V. Systematic optimization of exchange-correlation functionals. *J. Chem. Phys.* **1997**, *107*, 8554−8560.

(44) Grimme, S.; Antony, J.; Ehrlich, S.; Krieg, H. A consistent and accurate ab initio parametrization of density functional dispersion correction (DFT-D) for the 94 elements H-Pu. *J. Chem. Phys.* **2010**, *132*, 154104.

(45) Zhao, Y.; Truhlar, D. The M06 suite of density functionals for main group thermochemistry, thermochemical kinetics, noncovalent interactions, excited states, and transition elements: two new functionals and systematic testing of four M06-class functionals and 12 other functionals. *Theor. Chem. Acc.* **2008**, *120*, 215−241.

(46) Yanai, T.; Tew, D. P.; Handy, N. C. A new hybrid exchange-correlation functional using the Coulomb-attenuating method (CAM-B3LYP). *Chem. Phys. Lett.* **2004**, *393*, 51−57.

(47) Chai, J.-D.; Head-Gordon, M. Long-range corrected hybrid density functionals with damped atom-atom dispersion interactions. *Phys. Chem. Chem. Phys.* **2008**, *10*, 6615−6620.

(48) Larsen, H.; Hald, K.; Olsen, J.; Jørgensen, P. Triplet excitation energies in full configuration interaction and coupled-cluster theory. *J. Chem. Phys.* **2001**, *115*, 3015−3020.

(49) Watts, J. D.; Bartlett, R. J. Iterative and non-iterative triple excitation corrections in coupled-cluster methods for excited electronic states: The EOM-CCSDT-3 and EOM-CCSD($\tilde{T}$) methods. *Chem. Phys. Lett.* **1996**, *258*, 581−88.

(50) Epifanovsky, E.; Kowalski, K.; Fan, P.-D.; Valiev, M.; Matsika, S.; Krylov, A. I. On the electronically excited states of uracil. *J. Phys. Chem. A* **2008**, *112*, 9983−9992.

(51) Ghosh, D. Hybrid equation-of-motion coupled-cluster/effective fragment potential method: A route toward understanding photoprocesses in the condensed phase. *J. Phys. Chem. A* **2017**, *121*, 741−752.

(52) Plasser, F.; Wormit, M.; Dreuw, A. New tools for the systematic analysis and visualization of electronic excitations. I. Formalism. *J. Chem. Phys.* **2014**, *141*, 024106.

(53) Plasser, F.; Bäppler, S. A.; Wormit, M.; Dreuw, A. New tools for the systematic analysis and visualization of electronic excitations. I. Applications. *J. Chem. Phys.* **2014**, *141*, 024107.

(54) Plasser, F. Entanglement entropy of electronic excitations. *J. Chem. Phys.* **2016**, *144*, 194107.

(55) Johnson, J. R.; Jordan, K. D.; Plusquellic, D. F.; Pratt, D. W. High resolution $S_1 \leftarrow S_0$ fluorescence excitation spectra of the 1-and 2-hydroxynaphthalenes. Distinguishing the cis and trans rotamers. *J. Chem. Phys.* **1990**, *93*, 2258−2273.

(56) Hercules, D. M.; Rogers, L. B. Absorption and fluorescence spectra of some mono-and di-hydroxy naphthalenes. *Spectrochim. Acta* **1959**, *15*, 393−408.

(57) Bravaya, K. B.; Krylov, A. I. On the photodetachment from the green fluorescent protein chromophore. *J. Phys. Chem. A* **2013**, *117*, 11815−11822.

(58) Kamarchik, E.; Krylov, A. I. Non-Condon effects in one- and two-photon absorption spectra of the green fluorescent protein. *J. Phys. Chem. Lett.* **2011**, *2*, 488−492.

(59) Chantzis, A.; Laurent, A. D.; Adamo, C.; Jacquemin, D. Is the Tamm-Dancoff approximation reliable for the calculation of absorption and fluorescence band shapes? *J. Chem. Theory Comput.* **2013**, *9*, 4517−4525.

(60) Matsika, S.; Feng, X.; Luzanov, A. V.; Krylov, A. I. What we can learn from the norms of one-particle density matrices, and what we can't: Some results for interstate properties in model singlet fission systems. *J. Phys. Chem. A* **2014**, *118*, 11943−11955.

(61) Mewes, S. A.; Mewes, J.-A.; Dreuw, A.; Plasser, F. Excitons in poly (para phenylene vinylene): A quantum-chemical perspective based on high-level ab initio calculations. *Phys. Chem. Chem. Phys.* **2016**, *18*, 2548−2563.

(62) Bäppler, S. A.; Plasser, F.; Wormit, M.; Dreuw, A. Exciton analysis of many-body wave functions: Bridging the gap between the quasiparticle and molecular orbital pictures. *Phys. Rev. A* **2014**, *90*, 052521.

(63) Plasser, F.; Lischka, H. Analysis of excitonic and charge transfer interactions from quantum chemical calculations. *J. Chem. Theory Comput.* **2012**, *8*, 2777−2789.